Am J Physiol Regul Integr Comp Physiol 290: R114–R123, 2006.
First published October 13, 2005; doi:10.1152/ajpregu.00449.2005.

Quantitative 3D fluorescence technique for the analysis of en face preparations of arterial walls using quantum dot nanocrystals and two-photon excitation laser scanning microscopy

Dardo E. Ferrara,[1] Daiana Weiss,[1] Peter H. Carnell,[2] Ray P. Vito,[2] David Vega,[3] Xiaohu Gao,[4] Shuming Nie,[4] and W. Robert Taylor[1,5]

[1]*Division of Cardiology, Department of Medicine, Emory University, School of Medicine;* [2]*Woodruff School of Mechanical Engineering, Georgia Institute of Technology;* [3]*Division of Cardiothoracic Surgery. Department of Surgery, Emory University School of Medicine;* [4]*Departments of Biomedical Engineering and Chemistry, Emory University and Georgia Institute of Technology; and* [5]*Veterans Affairs Medical Center, Atlanta, Georgia*

Submitted 27 June 2005; accepted in final form 5 October 2005

Ferrara, Dardo E., Daiana Weiss, Peter H. Carnell, Ray P. Vito, David Vega, Xiaohu Gao, Shuming Nie, and W. Robert Taylor. Quantitative 3D fluorescence technique for the analysis of en face preparations of arterial walls using quantum dot nanocrystals and two-photon excitation laser scanning microscopy. *Am J Physiol Regul Integr Comp Physiol* 290: R114–R123, 2006. First published October 13, 2005; doi:10.1152/ajpregu.00449.2005.—Traditional imaging with one-photon confocal microscopy and organic fluorophores poses several challenges for the visualization of vascular tissue, including autofluorescence, fluorophore crosstalk, and photobleaching. We studied human coronary arteries (HCAs) and mouse aortas with a modified immunohistochemical (IHC) "en face" method using quantum dot (Qdot) bioconjugates and two-photon excitation laser scanning microscopy (TPELSM). We demonstrated the feasibility of multilabeling intimal structures by exciting multicolored Qdots with only one laser wavelength (750 nm). Detailed cell structures, such as the granular appearance of von Willebrand factor (VWF) and the subcellular distribution of endothelial nitric oxide synthase, were visualized using green dots (525 nm), even when the emission maximum of these Qdots overlapped that of tissue autofluorescence (510–520 nm). In addition, sensitive fluorescence quantification of vascular cell adhesion molecule 1 expression at areas of varying hemodynamics (intercostal branches vs. nonbranching areas) was performed in normal C57Bl/6 mice. Finally, we took advantage of the photostability of Qdots and the inherent three-dimensional (3D) resolution of TPELSM to obtain large z-stack series without photobleaching. This innovative en face method allowed simple multicolor profiling, highly sensitive fluorescence quantitation, and 3D visualization of the vascular endothelium with excellent spatial resolution. This is a promising technique to define the spatial and temporal interactions of endothelial inflammatory markers and quantify the effects of different interventions on the endothelium.

semiconductor nanocrystals; multiphoton microscopy; atherosclerosis; shear stress; vascular cell adhesion molecule 1

THE CHRONIC PROCESS OF ATHEROSCLEROSIS, in its different clinical forms, is the leading cause of morbidity and mortality in developed countries. Inflammation plays an important role in its pathogenesis, and the earliest molecular inflammatory events occur in the endothelium of conduit arteries. A vast amount of evidence supports the notion that risk factors, including hypercholesterolemia (17) and altered hemodynamic patterns (31), can cause endothelial cell (EC) activation leading to the expression of vascular cell adhesion molecule-1 (VCAM-1), which in turn, facilitates leukocyte adhesion and transendothelial migration.

Although our appreciation of the potential importance of these endothelial inflammatory changes has been growing (24), sensitive imaging techniques to assess these activated ECs, early in the course of atherosclerosis, are still lacking. The localization, morphology, size, and composition of atherosclerotic lesions in murine models are extensively studied in serial sections of the aortic sinus and in flat "en face" preparations of thoracic descending aorta (20, 25, 29, 37). However, neither one of these techniques is suitable for sensitive visualization of the spatial distribution of endothelial markers of activation. Moreover, there is a surprising scarcity of functional studies of the endothelium (1, 12, 14, 30), with only a few attempts made at studying the endothelial layer of these flat preparations using fluorescence confocal microscopy (12, 14). This is likely due to the fact that traditional fluorescence techniques with one-photon confocal microscopy and organic dyes pose several challenges for imaging vascular tissue, including tissue autofluorescence, fluorophore crosstalk, and photobleaching. Additionally, studies using static in vitro systems generate results that may be difficult to extrapolate to complex living organisms (6, 9). Consequently, there is a need for sensitive molecular imaging techniques to gather functional information on the complexity of gene expression, and the spatial and temporal interactions of protein expression in the endothelium.

Quantum dots (Qdots) are very small (<10 nm) inorganic fluorophores, typically made up of a cadmium selenide semiconductor core surrounded by a zinc sulfide shell. This core-shell complex can then be coated with a water-soluble polymer and finally attached to antibodies or other molecules, such as streptavidin to make them useful for immunohistochemistry (IHC) (4). These novel fluorescent tags have several unique

Address for reprint requests and other correspondence: W. Robert Taylor, Div. of Cardiology, Dept. of Medicine, Emory Univ. School of Medicine, Atlanta, GA 30322 (e-mail: wtaylor@emory.edu).

The costs of publication of this article were defrayed in part by the payment of page charges. The article must therefore be hereby marked "*advertisement*" in accordance with 18 U.S.C. Section 1734 solely to indicate this fact.

optical properties that make them very suitable for biological applications that require multiplexing and highly sensitive molecular detection (3, 11, 15). First, their narrow and symmetric emission reduces crosstalk and facilitates multilabeling. Second, their broad absorption spectra make possible the use of a single-excitation wavelength for multiplexing. Third, their high level of brightness and large Stokes shifts help deal with the common problem of tissue autofluorescence. Finally, their resistance to photobleaching makes them ideal probes for fluorescence quantitation.

Two-photon excitation (TPE) laser scanning microscopy (TPELSM) offers several advantages over one-photon confocal microscopy (41). Two optical features improve the signal-to-background ratio and three-dimensional (3D) spatial resolution. The first one, "localization of the excitation volume" is related to the principle of TPE and has been described elsewhere (7, 34). Briefly, this principle states that the excited state and emission of fluorescence can be achieved by the near simultaneous absorption of two longer-wavelength photons and because the amount of TPE depends on the square of the local illumination intensity, excitation is confined to a small volume around the focal point. Elsewhere along the beam pathway, excitation of out-of-focus fluorescence is not generated, and therefore a pinhole is never necessary. The second useful optical property is related to the fact that intrinsic tissue fluorophores (autofluorescence) have low TPE action cross sections (a quantitative measure of two-photon absorption) and blue shifts of their spectra (41). Finally, because the titanium-sapphire (TI:Sapphire) lasers currently used for TPELSM do not allow for rapid switching of excitation wavelengths, the use of Qdots, which have broad multiphoton absorption between 700 nm and 1,000 nm, offers a significant advantage for simultaneous excitation of multicolored Qdots with a single laser wavelength (15, 23).

Recently published studies have explored the combined use of TPE and Qdots for tracking tissue extravasation of multicolored cancer cells and the recruitment of bone marrow-derived cells to tumor microvasculature (36, 40). As yet, however, the potential of this technique for fluorescence quantitation and 3D reconstruction of highly scattering tissue, such as the arterial wall, has not been explored.

The aim of this study was to develop a sensitive yet simple fluorescence IHC en face method using Qdot bioconjugates and TPELSM to investigate intimal atherosclerotic changes in human coronary arteries and mouse aortas, especially at areas known to be exposed to different flow patterns. This method allowed us to obtain accurate multicolored labeling, reliable fluorescence quantitation of low-abundance antigens, and 3D visualization of the vascular endothelium.

MATERIALS AND METHODS

IHC reagents: primary antibodies and quantum dot bioconjugates. The primary antibodies (Abs) used were rat anti-mouse CD 31 [platelet endothelial cell adhesion modecule 1 (PECAM-1)] monoclonal IgG (1:500 dilution; BD PharMingen), biotinylated goat anti-mouse VCAM-1 affinity-purified IgG (1:50 dilution; R&D Systems), rat anti-mouse Mac-3 monoclonal IgG (1:200 dilution; BD PharMingen), rabbit polyclonal anti-von Willebrand factor (VWF; 1:100 dilution; DAKO), mouse monoclonal anti-smooth muscle actin (1:100 dilution; Sigma), and affinity purified rabbit polyclonal anti-endothelial nitric oxide synthase (e-NOS) (NOS3 at 1:500; Santa Cruz Biotechnology). Sections and tissue preparation were also treated with nonimmune primary antibodies to address the contribution of nonspecific Fc receptor-mediated binding. We used a nonimmune purified rat IgG2a κ (BD PharMingen) to control for PECAM 1 and Mac-3 Abs and a nonimmune biotinylated goat IgG (R&D Systems) as a control for VCAM-1. The chosen controls for e-NOS were a knockout mouse (negative control) and a blocking peptide (specificity control).

Qdot secondary antibodies were purchased from Quantum Dot. The following bioconjugates were used: Qdot 525 goat $(Fab')_2$ anti-rabbit IgG conjugate, Qdot 585 streptavidin conjugate, Qdot 655 goat $(Fab')_2$ anti-rat IgG conjugate and Qdot 655 goat $(Fab')_2$ anti-rabbit IgG conjugate. According to the manufacturer, the quantum yield of all these dots was $>$ 40–50%. We tested the peak and width of their emission spectra using the lambda stack function of the Zeiss LSM 510 META. As expected, their emission peaks were found to correspond to the advertised value and the width to be as narrow as 30 nm (full width at half maximum). A final concentration of 10–20 nM was satisfactory for most labeling experiments. Streptavidin/biotin blocking kit was obtained from Vector Laboratories. For nuclear counterstaining, Hoechst 33258 (1:1,000 dilution, Sigma) was used.

Animals. C57BL/6 and homozygous apoE-deficient (C57BL/6 background) male mice were purchased from the Jackson Laboratories. Mice of different ages (from 4 to 32 wk) were used in this study. Some were fed a standard chow diet (Purina Certified Rodent Chow 5001), and others were fed an atherogenic diet (Research Diets). The animals were housed and cared for according to the guidelines proposed by the National Institutes of Health for the care and use of experimental animals.

Mouse model of systemic endothelial activation. As a positive control for our quantitation studies, we used a previously described model of diffuse endothelial activation. In this model, widespread upregulation of endothelial inflammatory markers is achieved by an intraperitoneal injection of 100 μg of LPS from *Escherichia coli* (serotype 055:B5; BioChemika) given 5 h before euthanasia (13).

Harvest of human coronary arteries. Human coronary arteries were harvested, as previously described (35), from patients with end-stage heart failure undergoing heart transplantation at Emory University Hospital. Hearts were harvested during surgery, placed in ice-cold Krebs buffer, and transferred immediately to ice-cold Krebs buffer. Informed consent was obtained. The study protocol was approved by the Emory University Institutional Review Board.

Tissue preparation and immunohistochemical protocol. Animals were euthanized by CO_2 inhalation and the aortas were pressure-perfused at 100 mmHg with a cold 0.9% NaCl solution followed by pressure fixation with a 10% formalin solution. The thoracic descending aortas were then carefully dissected in situ by cutting off the intercostal branches and removing the adventitia. Finally, the aortas were opened longitudinally (following an anterior incision) from the point were the arch ends down to the renal arteries. Immediately afterward, the tissue was washed three times in PBS. The IHC staining procedure was done on a 24-well plate using volumes of ~500 μl per well. The washing steps were performed on the orbital shaker, and the incubations were performed on the rocker. A permeabilization step with 0.2% Triton X-100 for 15 min was done as needed, for intracellular and subendothelial targets. The tissue was then blocked with 2% BSA/5% goat serum in PBS for 1 h. An additional blocking step with streptavidin and biotin solutions was done when needed. The primary antibodies were diluted in blocking buffer and applied to the samples for overnight (16 h) incubation at 4°C. Additional washing steps were performed to remove first antibody excess. The Qdot-conjugated secondary antibody was diluted in 2%BSA and incubated for 1 h. The removal of the secondary Ab with a final wash was followed by nuclear counterstaining with Hoechst solution (1:1,000 dilutions) for 15 min. The specimens were then mounted on glass slides using Vectashield (Vector Laboratories). The human coronary arteries were treated in a similar way.

TPE microscopy. Tissue samples were analyzed and images collected using a Zeiss LSM 510 META two-photon microscope equipped with a near-infrared (NIR) Ti:Sapphire femtosecond laser (Mira 900 Ti:S; Coherent) tuned and mode-locked at 750 nm. For the majority of the experiments, a 40× (1.3 numerical aperture; Plan-Neofluor) oil immersion objective connected to an inverted Zeiss Axiovert 100 microscope was used, and the pinhole was left fully open. Additional magnification was performed by optical zoom in the scan head as needed. The beam pathway consisted of only one beam splitter (HFT KP 680). The separation of the emission signals was performed by acquisition of lambda stacks with posterior selection of reference spectra using the META detector. Forty-nanometer-wide filters were selected around the peak emission of the respective Qdots.

For 3D reconstruction, plaques and branches were imaged with the same objective that had a working distance of 170 μm at a resolution of 512 × 512 pixels. A stack of ~100 optical sections covered the entire depth of the mouse aortic wall. Mounting media and immersion oil had the same refractive index and no correction was made for Z-axis refractive index mismatch. Image processing for 3D visualization was done with Amira software (TGS series, Mercury Computer Systems).

Quantitation of fluorescence intensity. Fluorescence was quantified using the frequency histogram function of the LSM-510 examiner software. To measure the fluorescence of the region of interest (ROI) of the intercostal arteries, the entire image, using a standardized area, was analyzed. The ROI was centered on the orifice of the intercostal artery. For the region of undisturbed flow, the objective was moved to the anterior aspect of the aorta at the same level as the intercostal artery. Positioning was performed using the 4,6-diamidino 2-phenylindole settings only; thus we could not visualize any specific immunostaining that could potentially bias our selection of a microscopic field. Image capture of samples, prepared in a standardized way, was performed using the same confocal settings (33). Distorted and uneven portions of the samples were not considered for quantitation. As was the case with the intercostal arteries, we analyzed the entire microscopic field and did not specifically select a ROI within the field. Thus the ROI was in effect the entire microscopic field. A positive control sample (LPS-treated mouse) was imaged first and used to set the confocal settings (%transmission, detector gain) to avoid saturation. For each mouse sample, a negative control sample was used to establish the mean pixel intensity of the background signal. Mean background intensity was then digitally subtracted by applying the low threshold tool to the images, and the average signal intensity (mean fluorescence intensity in arbitrary units) was determined for each image. Because of statistical noise and to prevent skewing by extremely high outliers, we determined the highest intensity value to be 220 using the high-threshold tool (Fig. 1).

Statistical analysis and number of replications. For quantitative assays, results were expressed as means ± SE. Differences among groups were analyzed with two-way ANOVA using a commercially available software package (GraphPad Prism4). A P value of <0.05 was considered statistically significant. For all other qualitative results, the examples shown are representative of 10–15 replications from 5–10 animals.

RESULTS

Imaging endothelial cells with Qdots and TPELSM eliminates vascular autofluorescence. Because of the low TPE action cross sections of native organic fluorophores and the broad adsorption of Qdots, we hypothesized that the combined use of TPELSM and Qdots would allow the acquisition of confocal images without the need of subtracting digital algorhythms to eliminate the broadband vascular autofluorescence.

We found that the tissue autofluorescence was extremely low at the level of the endothelium. We tested three different channels along the visible spectrum (green, yellow-orange, and red), exciting with a 750-nm wavelength and using the same confocal settings (%transmission and detector gain) that would easily excite Qdots in the respective channels (Fig. 2). As a consequence, we found that the staining of endothelial targets with 525-nm Qdot bioconjugates was easy to detect, even though the broad "red tail" of the nuclear organic fluorophore (Hoechst) bled through the green channel. However, because of their completely different emission spectra, the crosstalk removal using the automatic component extraction (ACE) and spectral unmixing functions is straightforward (Fig. 3).

Therefore, TPE can improve resolution by increasing contrast because of its ability to reduce tissue autofluorescence. Moreover, the high quantum yield, large Stokes shifts, and narrow emission spectra of Qdots further allow easy detection by facilitating spectral separation (See *supplemental* Figs. 1–3 in http://ajpregu.physiology.org/cgi/content/full/00449.2005/DC1.

Multiplexing the aortic intima with Qdot bioconjugates. Crosstalk is a common problem in multifluorescence imaging with conventional confocal laser scanning microscopy. Multiple lasers are usually required to excite different colors of

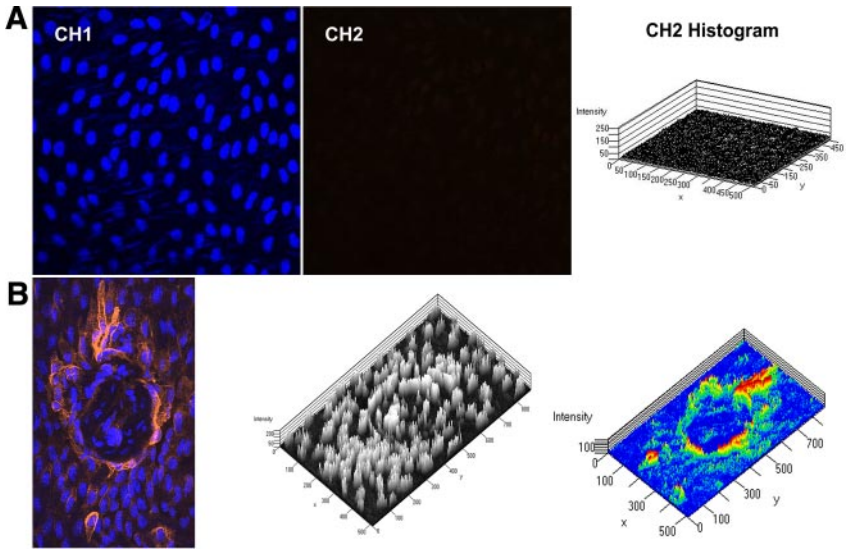

Fig. 1. Fluorescence quantification frequency histograms. *A*: negative control sample from a nonbranching area of a mouse descending aorta. Channel (CH) 1 (400–460 nm) corresponds to the nuclear staining Hoechst (blue). CH2 is for the detection of nanocrystals with a peak emission at 585 nm (560–600 nm). CH2 histogram shows very low levels of background fluorescence and no crosstalk from the blue channel that is excited with the same wavelength. *B*: positive sample on the left is the merged image of an intercostal branch of a normal C57Bl/6 mouse stained for vascular cell adhesion molecule-1 (VCAM-1). *Middle* and *right*: the pseudo-three dimensional (3D) frequency histograms for both channels (monochrome for Hoechst and rainbow for VCAM-1 stained with quantum dot (Qdots; QD) 585 nm streptavidin conjugate).

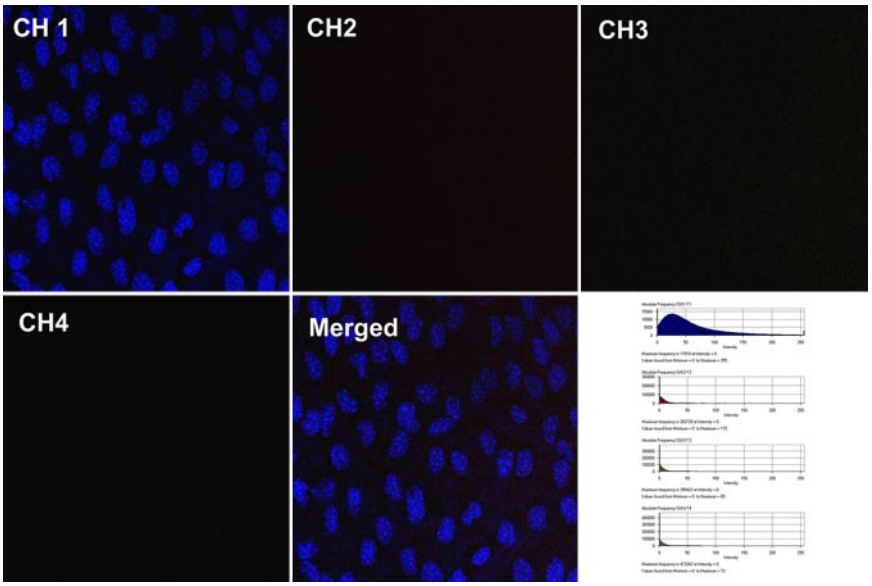

Fig. 2. Two-photon excitation of endothelial autofluorescence. Nonbranching region of a mouse thoracic aorta stained only with Hoechst (CH-1: 400–460 nm) to identify the endothelial layer. The autofluorescence in CH2 (635–675 nm), CH3 (560–600 nm), and CH4 (505–545 nm) is extremely low when excited at 750 nm and confocal settings that easily elicit Qdots fluorescence (%transmission $<$ 4 and detector gain $<$ 750). Histograms in the lower right panel show objective measurements of the intensities in the four channels.

organic fluorescent labels. In addition, standard fluorophores have broad emission spectra, which make their separation by band pass filters imperfect for multilabeling. In contrast, the visualization of multicolored Qdots with only one excitation wavelength is the method of choice because of their broad adsorption and narrow emission spectra.

We have found that multiplexing up to four fluorophores (nuclear staining and three endothelial markers) can be obtained without spectral overlapping (Fig. 4). Moreover, this was achieved with simple confocal settings (one excitation wavelength and only one dichroic mirror in the beam pathway).

Finally, it is worthy of note that achieving better spatial resolution between multicolored objects or molecules requires careful consideration of chromatic aberration (26). Therefore, in the case of Qdots that can be excited with one laser wavelength, aligned on the optical axis, the effects of chromatic aberration in the excitation pathway can be eliminated (22).

Quantitative analysis of VCAM-1 expression at areas exposed to different flow patterns in normal mice. Our en face technique has many of the idealized features required for image acquisition and quantification (fixed sample stained with a nonbleaching fluorophore that emit with a narrow emission spectra, minimal TPE autofluorescence, and optically selected filters using the lambda stack function and META detector) (8). Therefore, our goal was to prove the concept that the tightly regulated expression of VCAM-1 by flow could easily be quantified in normal animals (low-abundance target). We sought to answer the question of whether different flow patterns would have an effect on the expression of this inflammatory marker in the descending thoracic aorta of young (12-wk-old) C57Bl/6 mice. The descending aorta provides a large surface for analysis, but only small areas surrounding the intercostal artery ostia are prone to lesion development (25). This phenomenon makes the differences less well demarcated compared with the aortic arch.

For this quantitative study, images were obtained from regions around intercostal branches (high-probability regions, or HP) and from areas not prone to lesion formation chosen from the ventral wall of the descending thoracic aorta (low probability). For each mouse, 10 to 15 images were evaluated from each region.

We found that VCAM-1 expression was significantly upregulated around intercostal branches compared with nonbranching areas of the anterior aspect of the descending aorta in normal C57Bl/6 mice [19.54 $\pm$ 0.97 vs. 9.64 $\pm$ 0.78 arbitrary units (AU), $P < 0.001$] (Fig. 5, *A*, *B*, *E*). Because LPS has been shown to upregulate VCAM-1 expression, we used a model of diffuse endothelial inflammation as a positive control and to assess whether LPS would blunt the differences found between branches and nonbranching areas. We observed a statistically significant upregulation of VCAM-1 expression in both areas compared with untreated animals ($P < 0.0001$) (Fig. 5, *C–E*). The difference between HP and LP areas remained statistically significant but was partially blunted by LPS (42.95 $\pm$ 1.33 vs. 38.75 $\pm$ 0.99 AU).

3D reconstruction of atherosclerotic plaques and branching points. Confocal laser scanning microscopy has grown to become the tool of choice for 3D imaging. However, some limitations prevent one-photon confocal microscopy from becoming as popular as epifluorescence microscopy. One of these restrictions, photobleaching, has a negative impact on the collection of high-resolution z-stack images for 3D reconstruction. For these reasons, we sought to prove the concept that combining low-energy TPE—with its inherent deep penetration and 3D resolution—with highly stable Qdots would provide a very reliable tool for obtaining large z-stack imaging data files without losing image intensity.

Figure 6 depicts a 3D reconstruction of an atherosclerotic lesion that has grown to cover an intercostal branch of a 6-mo-old apolipoprotein (apo)E knockout (KO) mouse. This is a common phenomenon that starts around 16 wk of age and affects $>$ 50% of the branches at 24 wk, even in apoE KO mice fed a normal chow diet. Of note is the striking EC disarray at the dome of the lesion.

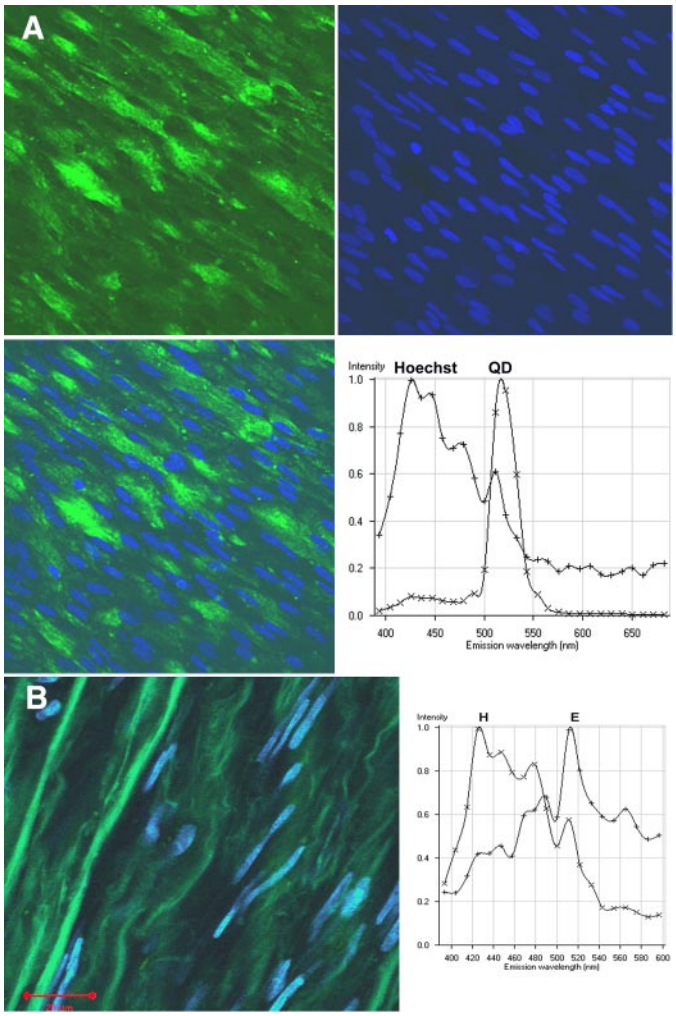

Fig. 3. Nonbranching area of a human circumflex artery. *A*: endothelium was targeted with a polyclonal rabbit anti-von Willebrand factor IgG and stained with Qdot 525 nm (green) goat anti-rabbit IgG conjugate. Nuclei were counterstained with Hoechst (blue). Notice the wide emission spectrum of the organic fluorophore (H) with its red tail partially overlapping with the narrow and symmetric emission of the green QD. However, the crosstalk was readily eliminated with automatic component extraction (ACE) and multichannel unmixing (see *Imaging endothelial cells with Qdots and TPELSM eliminates vascular autofluorescence*). *B*: same artery was imaged at the media level. The lambda stack function was used to obtain the autofluorescence spectrum of the elastin fibers (E) and smooth muscle cells. The %laser transmission was 3–5 times higher than for Fig. 3*A*. Compare the wide and overlapping spectra of (H) and (E) with that of QD shown in Fig.3*A*. Again, spectral separation was performed using ACE and linear unmixing.

The supplementary movie available online shows the AMIRA 3D reconstruction.

Imaging within deep-scattering vascular tissue with TPELSM. To confirm the penetration depth of NIR TPE and to study the diffusion of Qdot bioconjugates within the vascular wall, we attempted to target macrophages and smooth muscle cells of mouse aortas and human coronary arteries.

As shown in supplemental Fig. 4 at http://ajpregu.physiology.org/cgi/content/full/00449.2005/DC1, we were able to image SMCs' nuclei stained with Hoechst down to 100 μm in depth. This is consistent with prior reports comparing TPELSM with one-photon confocal microscopy to image the vascular wall (39). However, staining the smooth muscle cell (SMC) layer targeting α-actin was not possible. SMCs were easily stained at the edge of the tissue samples, but the label was not detected further into the tissue (not shown). In contrast, we found surface macrophage antigens easier to label in the intima using permeabilization with Triton X-100 (Fig. 4*A*). Additionally, we demonstrated that the cellular membrane is not an obstacle for Qdots by staining different intracellular endothelial markers (VWF, eNOS) (Fig. 3*A* and 4*B*). Nonetheless, the penetration of these nanoparticles was, in general, poor beyond the superficial part of the intima. Basal membranes, thick fibrous caps, and the lamina elastica interna are the most likely barriers for the diffusion of these small particles.

DISCUSSION

The current study demonstrates that our novel fluorescence en face technique has considerable advantages (no autofluorescence, sensitive quantitation, and 3D reconstruction) over traditional methods, especially for examining early inflammatory changes of the endothelium (low target levels) at sites exposed to different flow patterns.

The endothelium is continuously exposed to numerous atherogenic factors such as hyperlipidemia, the diabetic milieu, and altered patterns of shear stress. The expression of adhesion molecules and leukocyte recruitment are early features of atherogenesis. Understanding these early events and how ECs respond to different interventions will help discover potential new approaches to treat this devastating disease.

The conventional approach to investigating these events is limited to in vitro models using cultured ECs. The biochemical analysis of these cellular homogenates provides very useful information on the type and relative amount of biomolecules (mRNA, proteins) present under different experimental settings (6, 9). However, a further, crucial step is needed to link this high-throughput genomic and proteomic information to the behavior of these cells in vivo, to finally understand the complex effects of diverse regulatory mechanisms. Therefore, there is a demand for sensitive imaging tools to visualize and quantify early dynamic atherosclerotic changes ex vivo to finally test the concepts and conclusions drawn from in vitro experiments.

IHC detection of low-level antigen expression in the vascular tissue is a complicated task due to interference by different native compounds (NADH, collagen, elastin, and others) that exhibit fluorescence over a wide spectrum of wavelengths. Indeed, one of the major shortcomings of epifluorescence and one-photon confocal microscopy in the analysis of vascular tissue is related to this autofluorescence that decreases contrast and makes the use of green fluorophores almost impossible. Diverse techniques have been used to overcome this problem, including photobleaching with UV irradiation and various chemical modifications (2, 19). Furthermore, a common approach used in confocal microscopy, which involves the digital subtraction of the emission obtained with different filters, adds one more complex step to the process of image acquisition. In our en face method, the problematic "green" vascular autofluorescence with poor contrast is solved by using highly fluorescent Qdots in combination with TPELSM. Most tissues have reduced absorption in the near-infrared part of the spectrum; thus TPE can effectively exploit the tissues' "optical window" at 700–1,000 nm (21). Indeed, the probability of TPE of Qdots

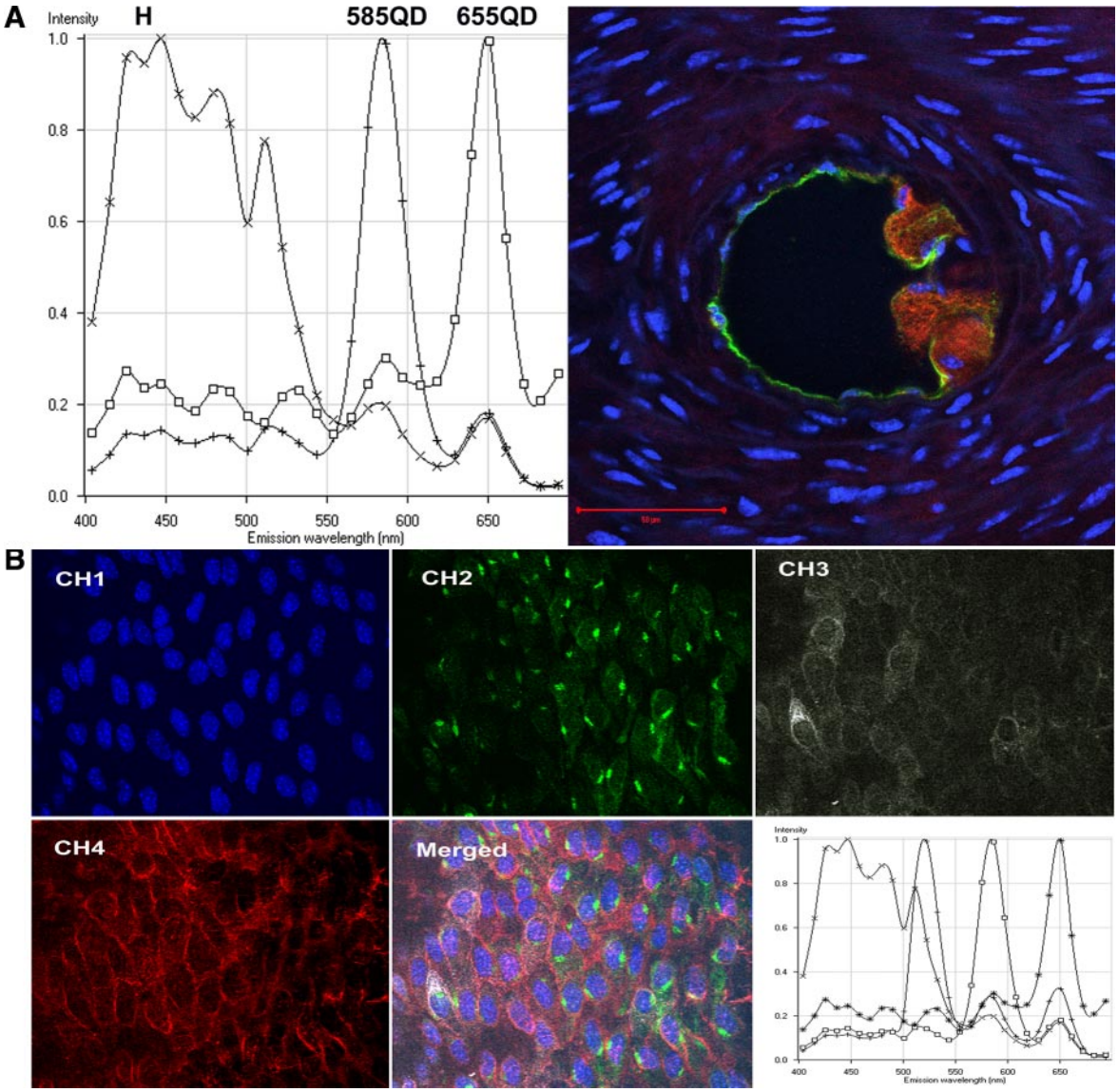

Fig. 4. Multiplexing with one excitation wavelength. *A*: intercostal branch of an apolipoprotein E knockout (apoE KO) mouse sectioned at the level of the media. Endothelial cells were targeted with a biotinylated anti-VCAM-1 Ab and Qdot-585nm (585QD) streptavidin conjugates (pseudocolored green for contrast). Macrophages were stained with a monoclonal rat anti-mouse Ab. (Mac-3) and Qdot-655nm (655QD) [goat anti-rat IgG conjugate (red)]. Nuclear counterstaining was done with Hoechst (blue). The elongated nuclei correspond to smooth muscle cells. The emission spectra of the fluorophores are on the left. Only one wavelength (750 nm) was used to excite all three fluorophores. *B*: nonbranching area of a normal C57Bl/6 mouse. Endothelial cell nuclei were stained with Hoechst (CH1). eNOS staining is shown in green (CH2). CH3 shows isolated cells that stain positive for VCAM-1 targeted with 585QD nm streptavidin bioconjugates (in white for contrast). Finally, the red channel (CH4) shows the typical membrane distribution of platelet endothelial cell adhesion molecule-1 marked with 655QD nm IgG conjugate. *Bottom right*: emission spectra of these four fluorophores.

is six orders of magnitude higher than with native molecules, such as NADH (23). Moreover, another property of Qdots (large Stokes shifts) also provides a means to improve the signal-to-noise ratio (contrast) and overcome the difficulty of background autofluorescence to which other fluorescent tags are still subject.

Even though spatial resolution beyond the diffraction limit of light is not necessarily enhanced with TPE, the effective resolution achieved in confocal microscopy is a function of several factors, including contrast (41). Therefore, the combination of Qdots and TPE can greatly increase resolution in scattered samples by improving the signal-to-noise ratio. This enhancement in contrast might also have another explanation. In standard one-photon laser scanning microscopy, the excitation wavelength is spectrally close to the fluorescence emission of organic fluorophores. There is a consequent decline in sensitivity with the use of filters to eliminate the leak-through of the excitation emission into the detection channel. In contrast, the NIR excitation wavelength used in TPELSM is much farther from the emission spectra, and efficient filters can be applied to eliminate the excitation with minimal attenuation of the signal.

We have also confirmed that Qdots are ideal fluorochromes for multicolor fluorescent detection, especially in experiments where accurate localization is necessary. This high throughput can provide researchers with the capability of rapid profiling.

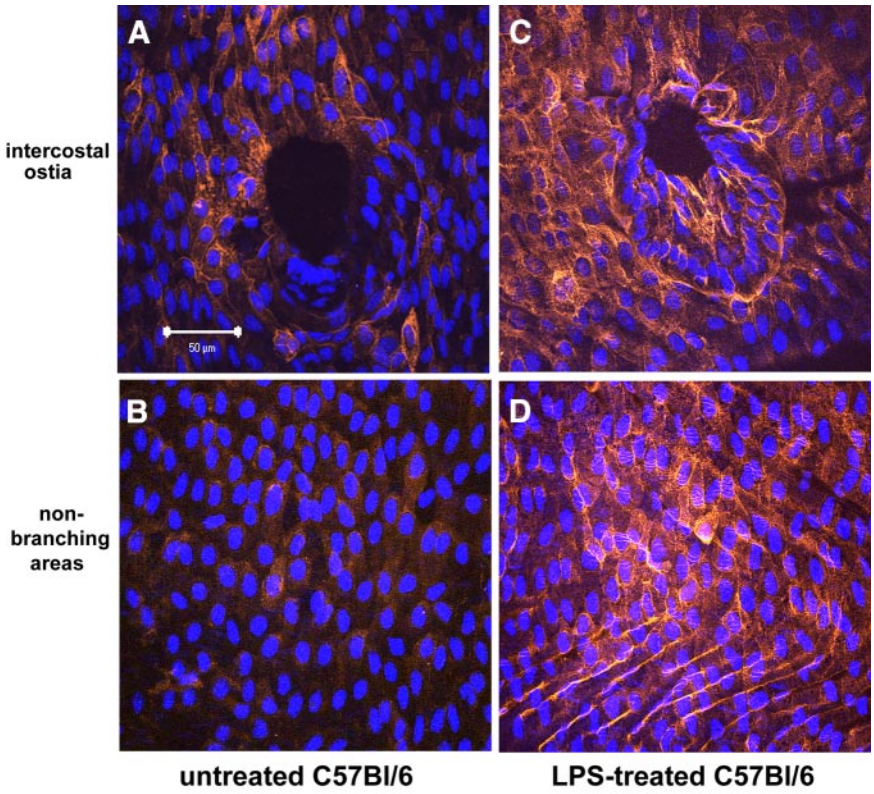

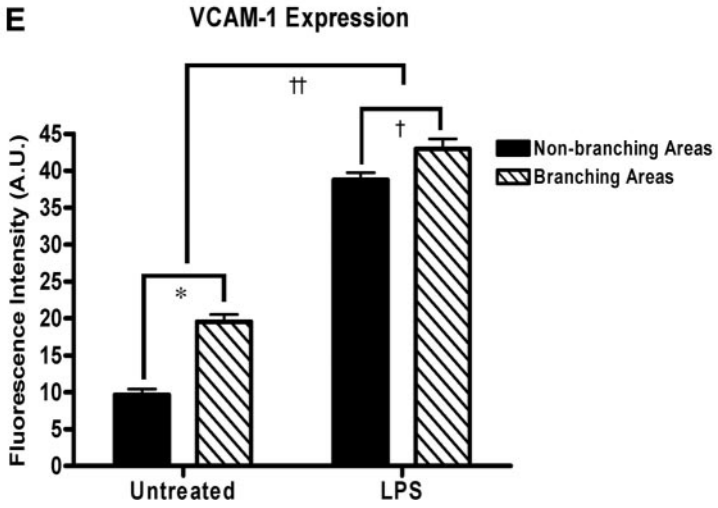

Fig. 5. Differential VCAM-1 expression in relation to flow dynamics and LPS treatment in 12-wk-old normocholesterolemic C57Bl/6 mice. Approximately 10–15 areas per region (intercostal branches vs. nonbranching areas) were imaged per animal (n = 2–3 per group). VCAM-1 was significantly upregulated at branched areas compared with straight parts in untreated C57Bl/6 (*$P < 0.001$) (*A*, *B*, *E*). Important upregulation was seen after 5 h of LPS treatment (100 μg ip) compared with the untreated group as a whole (††$P < 0.0001$) with partial blunting of the difference between regions (†$P < 0.01$). Values represent relative fluorescence intensity in arbitrary units (AU) and are expressed as means ± SE.

We have shown that several endothelial markers can be visualized simultaneously (multiplexing) with one excitation wavelength. We have only determined the feasibility of multilabeling with up to four fluorophores because we used an indirect (two-step) IHC procedure to easily test for nonspecific binding with nonimmune primary Abs. However, it is conceivable to increase this number substantially by means of direct conjugation of functionalized Qdots combined with recently developed software functions (ACE and linear unmixing). Finally, multiplexing Qdots of different colors with one excitation wavelength is a way of obtaining better resolved colocalization, by decreasing chromatic aberration in the excitation pathway (27).

Although making relative intensity measurements is in theory a simple task, the detection of low-abundance targets with even the best organic dye is a challenge. The weak signals and photobleaching make it very difficult to reliably record and quantify staining. We believe that our method at least partially overcomes this problem and provides an accurate way of quantifying relatively low levels of protein expression on the aortic endothelial surface, including the regions around its branches. The early differential expression of VCAM-1 that we have detected in the descending aorta of normocholesterolemic C57Bl/6 mice has not been previously reported. Nakashima et al. (30) have studied the differential expression of VCAM-1

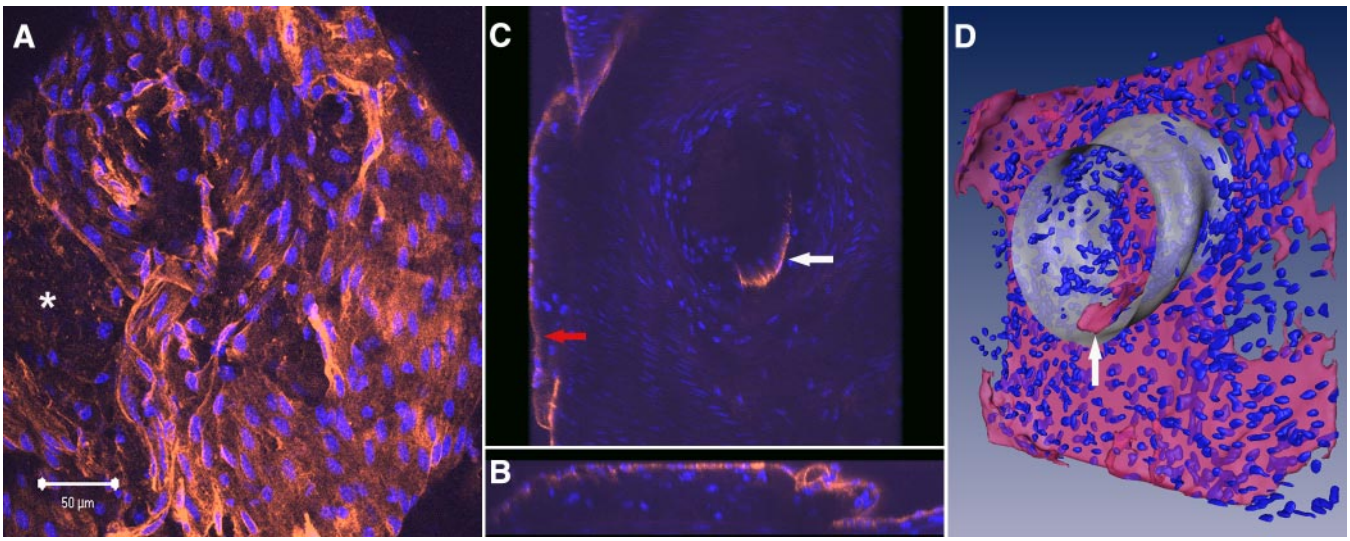

Fig. 6. 3D reconstruction of an intercostal branch occluded by an atherosclerotic lesion. A z-stack file of ~100 images was collected in 1 h. Individual components were reconstructed separately in AMIRA after preprocessing in Matlab. Positive endothelial VCAM-1 signal (585QD nm, orange) was used for surface reconstruction of the plaque and the occluded intercostal branch. Cell nuclei were identified using Hoechst counterstaining (blue). Small objects (<100 μm^3) were not considered nuclei and were excluded from the reconstruction. *A*: notice the endothelial cell disorganization over the plaque with areas of missing endothelium (*), X-Z 90° projection of the plaque (*B*), and Y-Z 45° pseudo-3D projection of the plaque obtained with the LSM 510 examiner software (*C*). The plaque surface (red arrow) and the partially occluded ostium (white arrow) are seen from below. This is the mirror image of *D*. *D*: Amira 3D reconstruction. The almost completely occluded lumen of the intercostal artery was hand-segmented based on a discernable pattern of VCAM-1 fluorescence (white arrow). This representation of the true occluded lumen was compared with the pattern of circumferentially aligned smooth muscle cells (original lumen).

using the en face method with gold nanoparticles and reflected light. Although they have provided a detailed qualitative description of the expression of this adhesion molecule in hypercholesterolemic apoE KO mice, their technique was not sensitive enough to detect the subtle but certain upregulation of VCAM-1 at lesion-prone areas of normocholesterolemic C57BL/6 mice. Furthermore, the need for silver intensification of the reaction makes quantification very difficult (32). Iiyama et al. (14) have also focused on VCAM-1 and attempted to quantify its differential expression in normal aortas. They used one-photon confocal microscopy along with organic fluorophores to compare the expression of this molecule at areas with different probabilities of lesion formation of the aortic arch in C57BL/6 mice. However, because photobleaching during sample preparation and image acquisition is almost unavoidable and makes quantitation unreliable, high variability prevented the analysis of pooled data and group comparisons. Additionally, these researchers did not perform a quantitative analysis of the thoracic descending aorta of these control mice fed normal chow. Finally, they have also acknowledged that some results might have been an artifact because the accuracy of quantifying low fluorescent signals is decreased as a result of background fluorescence (12).

Resistance of Qdots to bleaching over long periods coupled with the inherent 3D resolution of TPELSM is especially useful for obtaining well-contrasted z-sections. Actually, the TPE action cross sections of these nanocrystals have been found to remain stable for up to 9 mo (23). Recently, Tokumasu et al. (38) have shown that using Qdots for 3D reconstruction of human erythrocytes provides excellent resolution without the problem of photobleaching.

Here, we have also confirmed that our technique is well suited for 3D reconstruction of the vascular wall at the level of atherosclerotic plaques and intercostal branches.

We believe that the main disadvantage of this technique is the difficult and unreliable diffusion of these nanoparticles through the intimal layers, with a complete inability to stain the vascular media. This is likely due to the size of Qdot-bioconjugates that approach the size of a large protein, even when functionalized with $(Fab')_2$ fragments, as is the case with current commercially available conjugates. One way to partially overcome this problem is the functionalization with smaller ligands, such as peptides. However, we believe that the difficulty targeting subendothelial structures will persist. Moreover, concerns have been raised regarding the difficulty of washing away probes that are in excess in the cytoplasm (28). In this respect, we have not detected nonspecific staining even using Triton X-100 to permeabilize the tissue for up to 15 min and incubating with Qdot bioconjugates for up to 2 h. Nevertheless, we have seen that prolonged exposure to the detergent and conjugates increases the chances of cytoplasmic entrapment.

Obviously, one additional drawback of our technique is that it cannot provide longitudinal analyses at different time points. Because it is an ex vivo study, the number of animals required for evaluating the effects of interventions is larger compared with recently developed MRI-based molecular imaging techniques, which may offer the ability to scan the same animal before and after the application of a particular intervention (16). However, the recent emergence of both NIR fluorescence molecular tomography (5) and stable NIR Qdots (18) may soon allow quantitative 3D fluorescence imaging in vivo. Alternatively, targeted Qdots functionalized with polyethylene glycol

(10) or cells loaded with nanocrystals may help define endothelial or monocyte behaviors using in vivo imaging of smaller blood vessels with TPELSM (23, 36).

In summary, the present study has shown a highly sensitive yet easy-to-use 3D en face technique that is suitable for detecting and quantifying very early EC changes at areas prone to develop atherosclerosis. The combination of bright and stable Qdots along with the intrinsic 3D resolution of TPELSM has made possible excellent spatial discrimination of fluorescence signals in a strongly scattering biological specimen. This is a promising method for the investigation of the dynamics of endothelial markers in genetically manipulated animals and of the effects of different experimental interventions in vivo.

ACKNOWLEDGMENTS

We acknowledge Deborah Martinson for providing the IHC protocol to stain mouse aortas and for continuous technical support. We are also grateful to Howard Rees for sharing his expertise in TPELSM.

GRANTS

This work was supported by the National Institutes of Health Grants R-O1-L70531 and UO-1-NH-080711.

REFERENCES

1. **Azuma K, Watada H, Niihashi M, Otsuka A, Sato F, Kawasumi M, Shimada S, Tanaka Y, Kawamori R, and Mitsumata M.** A new en face method is useful to quantitate endothelial damage in vivo. *Biochem Biophys Res Commun* 309: 384–390, 2003.
2. **Baschong W, Suetterlin R, and Laeng RH.** Control of autofluorescence of archival formaldehyde-fixed, paraffin-embedded tissue in confocal laser scanning microscopy (CLSM). *J Histochem Cytochem* 49: 1565–1572, 2001.
3. **Chan WC, Maxwell DJ, Gao X, Bailey RE, Han M, and Nie S.** Luminescent quantum dots for multiplexed biological detection and imaging. *Curr Opin Biotechnol* 13: 40–46, 2002.
4. **Chan WCW and Nie SM.** Quantum dot bioconjugates for ultrasensitive nonisotopic detection. *Science* 282: 2016–2018, 1998.
5. **Chen J, Tung CH, Mahmood U, Ntziachristos V, Gyurko R, Fishman MC, Huang PL, and Weissleder R.** In vivo imaging of proteolytic activity in atherosclerosis. *Circulation* 105: 2766–2771, 2002.
6. **Dai G, Kaazempur-Mofrad MR, Natarajan S, Zhang Y, Vaughn S, Blackman BR, Kamm RD, Garcia-Cardena G, and Gimbrone MA Jr.** Distinct endothelial phenotypes evoked by arterial waveforms derived from atherosclerosis-susceptible and -resistant regions of human vasculature. *Proc Natl Acad Sci USA* 101: 14871–14876, 2004.
7. **Denk W, Strickler JH, and Webb WW.** Two-photon laser scanning fluorescence microscopy. *Science* 248: 73–76, 1990.
8. **Dobrucki JW.** Confocal microscopy: quantitative analytical capabilities. *Methods Cell Biol* 75: 41–72, 2004.
9. **Donners MM, Verluyten MJ, Bouwman FG, Mariman EC, Devreese B, Vanrobaeys F, van Beeumen J, van den Akker LH, Daemen MJ, and Heeneman S.** Proteomic analysis of differential protein expression in human atherosclerotic plaque progression. *J Pathol* 206: 39–45, 2005.
10. **Gao X, Cui Y, Levenson RM, Chung LW, and Nie S.** In vivo cancer targeting and imaging with semiconductor quantum dots. *Nat Biotechnol* 22: 969–976, 2004.
11. **Gao X and Nie S.** Molecular profiling of single cells and tissue specimens with quantum dots. *Trends Biotechnol* 21: 371–373, 2003.
12. **Hajra L, Evans AI, Chen M, Hyduk SJ, Collins T, and Cybulsky MI.** The NF-kappa B signal transduction pathway in aortic endothelial cells is primed for activation in regions predisposed to atherosclerotic lesion formation. *Proc Natl Acad Sci USA* 97: 9052–9057, 2000.
13. **Henninger DD, Panes J, Eppihimer M, Russell J, Gerritsen M, Anderson DC, and Granger DN.** Cytokine-induced VCAM-1 and ICAM-1 expression in different organs of the mouse. *J Immunol* 158: 1825–1832, 1997.
14. **Iiyama K, Hajra L, Iiyama M, Li H, DiChiara M, Medoff BD, and Cybulsky MI.** Patterns of vascular cell adhesion molecule-1 and intercellular adhesion molecule-1 expression in rabbit and mouse atherosclerotic lesions and at sites predisposed to lesion formation. *Circ Res* 85: 199–207, 1999.
15. **Jaiswal JK and Simon SM.** Potentials and pitfalls of fluorescent quantum dots for biological imaging. *Trends Cell Biol* 14: 497–504, 2004.
16. **Kelly KA, Allport JR, Tsourkas A, Shinde-Patil VR, Josephson L, and Weissleder R.** Detection of vascular adhesion molecule-1 expression using a novel multimodal nanoparticle. *Circ Res* 96: 327–336, 2005.
17. **Khan BV, Parthasarathy SS, Alexander RW, and Medford RM.** Modified low-density lipoprotein and its constituents augment cytokine-activated vascular cell adhesion molecule-1 gene expression in human vascular endothelial cells. *J Clin Invest* 95: 1262–1270, 1995.
18. **Kim S, Lim YT, Soltesz EG, De Grand AM, Lee J, Nakayama A, Parker JA, Mihaljevic T, Laurence RG, Dor DM, Cohn LH, Bawendi MG, and Frangioni JV.** Near-infrared fluorescent type II quantum dots for sentinel lymph node mapping. *Nat Biotechnol* 22: 93–97, 2004.
19. **Kingsley K, Carroll K, Huff JL, and Plopper GE.** Photobleaching of arterial autofluorescence for immunofluorescence applications. *Biotechniques* 30: 794–797, 2001.
20. **Klinkner AM, Bugelski PJ, Waites CR, Louden C, Hart TK, and Kerns WD.** A novel technique for mapping the lipid composition of atherosclerotic fatty streaks by en face fluorescence microscopy. *J Histochem Cytochem* 45: 743–753, 1997.
21. **Konig K.** Multiphoton microscopy in life sciences. *J Microsc* 200: 83–104, 2000.
22. **Lacoste TD, Michalet X, Pinaud F, Chemla DS, Alivisatos AP, and Weiss S.** Ultrahigh-resolution multicolor colocalization of single fluorescent probes. *Proc Natl Acad Sci USA* 97: 9461–9466, 2000.
23. **Larson DR, Zipfel WR, Williams RM, Clark SW, Bruchez MP, Wise FW, and Webb WW.** Water-soluble quantum dots for multiphoton fluorescence imaging in vivo. *Science* 300: 1434–1436, 2003.
24. **Libby P.** Inflammation in atherosclerosis. *Nature* 420: 868–874, 2002.
25. **McGillicuddy CJ, Carrier MJ, and Weinberg PD.** Distribution of lipid deposits around aortic branches of mice lacking LDL receptors and apolipoprotein E. *Arterioscler Thromb Vasc Biol* 21: 1220–1225, 2001.
26. **Michalet X, Kapanidis AN, Laurence T, Pinaud F, Doose S, Pflughoefft M, and Weiss S.** The power and prospects of fluorescence microscopies and spectroscopies. *Annu Rev Biophys Biomol Struct* 32: 161–182, 2003.
27. **Michalet X, Lacoste TD, and Weiss S.** Ultrahigh-resolution colocalization of spectrally separable point-like fluorescent probes. *Methods* 25: 87–102, 2001.
28. **Michalet X, Pinaud FF, Bentolila LA, Tsay JM, Doose S, Li JJ, Sundaresan G, Wu AM, Gambhir SS, and Weiss S.** Quantum dots for live cells, in vivo imaging, and diagnostics. *Science* 307: 538–544, 2005.
29. **Millonig G, Niederegger H, and Wick G.** Analysis of the cellular composition of the arterial intima with modified en face techniques. *Lab Invest* 81: 639–641, 2001.
30. **Nakashima Y, Raines EW, Plump AS, Breslow JL, and Ross R.** Upregulation of VCAM-1 and ICAM-1 at atherosclerosis-prone sites on the endothelium in the ApoE-deficient mouse. *Arterioscler Thromb Vasc Biol* 18: 842–851, 1998.
31. **Nerem RM, Alexander RW, Chappell DC, Medford RM, Varner SE, and Taylor WR.** The study of the influence of flow on vascular endothelial biology. *Am J Med Sci* 316: 169–175, 1998.
32. **Ogiwara N, Usuda N, Yamada M, Johkura K, Kametani K, and Nakazawa A.** Quantification of protein A-gold staining for peroxisomal enzymes by confocal laser scanning microscopy. *J Histochem Cytochem* 47: 1343–1349, 1999.
33. **Pawley J.** The 39 steps: a cautionary tale of quantitative 3-D fluorescence microscopy. *Biotechniques* 28: 884–886, 888, 2000.
34. **Rubart M.** Two-photon microscopy of cells and tissue. *Circ Res* 95: 1154–1166, 2004.
35. **Sorescu D, Weiss D, Lassegue B, Clempus RE, Szocs K, Sorescu GP, Valppu L, Quinn MT, Lambeth JD, Vega JD, Taylor WR, and Griendling KK.** Superoxide production and expression of nox family proteins in human atherosclerosis. *Circulation* 105: 1429–1435, 2002.
36. **Stroh M, Zimmer JP, Duda DG, Levchenko TS, Cohen KS, Brown ED, Scadden DT, Torchilin VP, Bawendi MG, Fukumura D, and Jain**

RK. Quantum dots spectrally distinguish multiple species within the tumor milieu in vivo. *Nat Med* 11: 678–682, 2005.

37. **Tangirala R, Rubin E, and Palinski W.** Quantitation of atherosclerosis in murine models: correlation between lesions in the aortic origin and in the entire aorta, and differences in the extent of lesions between sexes in LDL receptor-deficient and apolipoprotein E-deficient mice. *J Lipid Res* 36: 2320–2328, 1995.
38. **Tokumasu F and Dvorak J.** Development and application of quantum dots for immunocytochemistry of human erythrocytes. *J Microsc* 211: 256–261, 2003.
39. **van Zandvoort M, Engels W, Douma K, Beckers L, Oude Egbrink M, Daemen M, and Slaaf DW.** Two-photon microscopy for imaging of the (atherosclerotic) vascular wall: a proof of concept study. *J Vasc Res* 41: 54–63, 2004.
40. **Voura EB, Jaiswal JK, Mattoussi H, and Simon SM.** Tracking metastatic tumor cell extravasation with quantum dot nanocrystals and fluorescence emission-scanning microscopy. *Nat Med* 10: 993–998, 2004.
41. **Zipfel WR, Williams RM, and Webb WW.** Nonlinear magic: multiphoton microscopy in the biosciences. *Nat Biotechnol* 21: 1369–1377, 2003.